NONCONFORMAL PERTURBATIONS OF $z \mapsto z^2 + c$: THE 1:3 RESONANCE

H. BRUIN & M. VAN NOORT

ABSTRACT. We study a family of non-conformal maps of the plane, as a perturbation of the quadratic map $z \mapsto z^2 + c$. In particular, a neighborhood in phase-parameter space of the 1:3 resonance of the unperturbed map is analyzed, by theoretical and numerical means, mostly in a local setting, but some more global aspects are discussed as well.

Certain topological constructions, like the Mandelbrot and Julia sets, and external rays, can be carried through to the nonanalytic setting. Other familiar properties of the quadratic map, like the number and possible types of periodic points, are lost under the perturbation.

A bifurcation analysis shows complicated dynamics, where the 1:3 resonance point as well as cusp and Bogdanov-Takens points act as organizing centers. Arnol'd tongues and invariant circles – originating from Neimarck-Sacker bifurcations – also play an important role in structuring the dynamics. Finally, we discuss a planar vector field approximation of the family of maps that can explain part of these phenomena.

1. INTRODUCTION

The quadratic family $z \mapsto z^2 + c$ on the complex plane has been extremely well studied, and its "bifurcation diagram", the *Mandelbrot set* $\mathcal{M}$ is famous even outside mathematics. Our understanding of the quadratic family depends largely on its conformal nature and the tools from complex analysis that apply to it. Perturbations, especially nonconformal perturbations, of this family are much less understood. In Bielefeld et al. [4], the family

$$f_{\alpha,c}(z) = |z|^{2\alpha-2} z^2 + c \tag{1}$$

is proposed; it still has the global structure of a two-fold covering map of the plane with a single critical point at the origin, while its conformal structure is lost for $\alpha \neq 1$. For $\alpha \neq 1$, Mandelbrot sets $\mathcal{M}_\alpha$, being the c-locus of connected filled-in Julia sets can still be defined, and for $\alpha \approx 1$ roughly have the same shape as the standard Mandelbrot set. If the attention is restricted to the "main cardioid" and the (hyperbolic) components directly attached to it, it is a general observation that for $\alpha > 1$, these components tend to sink into the main cardioid (allowing coexistence of attractors), while for $\alpha < 1$, the components seem to detach themselves from the main cardioid, see [4, Figure 13].

The boundary of the main cardioid can be computed explicitly for $\alpha > 1/2$, see formula (2). For the conformal case ($\alpha = 1$) the bifurcations at the boundary of the cardioid are well-understood; they occur to the "central" fixed point and for multipliers at resonance

2000 *Mathematics Subject Classification.* Primary: 37G15 - Secondary: 37G05, 37F45, 70K30.

HB was supported by a fellowship of the Royal Netherlands Academy of Arts and Sciences (KNAW). The research was largely carried out at the University of Groningen.

($\mu = e^{2\pi ip/q}$), they are known as Leau-Fatou bifurcations. Bielefeld et al. [4] give a thorough analysis for $\alpha \approx 1$ of the bifurcation of the central fixed point near multiplier $\mu = 1$ (the root of the main cardioid) and multiplier $\mu = -1$ (the period doubling), while Peckham et al. [22, 23] give similar results for a slightly different family. The bifurcation structure at other multipliers is more conjectural.

In this paper we intend to carry out a thorough analysis of the bifurcations near the 1:3 resonance, i.e., multiplier $e^{2\pi i/3}$, where the nonanalytic family is considered as an unfolding of the analytic case $\alpha = 1$ in the space of C^∞ maps on the punctured plane $\mathbb{R}^2 \setminus \{0\}$. Obviously, (1) is not the most general family to study the (local and global) bifurcations, since there is a single critical point. Generic, but local, perturbations are studied in [22, 23], whereas Nien, [21], involves the critical set in an analysis of quadratic maps. For our system, $\alpha - 1$ plays the role of a small perturbation parameter, and our interest lies with those parts of the dynamics that are present for arbitrarily small $\alpha - 1$. Firstly this involves an analysis of the local bifurcations, using both numerical tools and general bifurcation theory. It is important to note that Leau-Fatou bifurcations or the presence of Siegel disks are not generic in the context of C^∞ maps on the plane. On the other hand, saddles and hyperbolic invariant circles, and consequently saddle-node and Neimarck-Sacker bifurcations are possible only for $\alpha \neq 1$.

Secondly, more global aspects, such as the dynamics of invariant circles or the critical point, are studied by topological means, again backed up by numerical calculations. Many of the constraints on analytic maps do not hold in the real setting. For example, there can be more attractors than critical points (so in our case, more than one), and the Julia set need not coincide with the boundary of the basin of ∞. However, other, more topological properties are still true.

1.1. **Method and results.** In the conformal case, the Leau-Fatou bifurcation at the 1:3 resonance involves a period three orbit passing through the fixed point, exchanging stability at the bifurcation point. The corresponding Julia set is known as the fat rabbit (of Douady). Under perturbation ($\alpha \neq 1$), this bifurcation falls apart in a complicated configuration of saddle-node and Neimarck-Sacker bifurcations (i.e., the discrete time version of Hopf bifurcations) of period three points. The bifurcations are organized by some codimension 2 Bogdanov-Takens and cusp points. The configurations for $\alpha < 1$ and $\alpha > 1$ are different. In both cases the bifurcation pattern is generic in the context of C^∞ maps on the real plane.

Of special interest are the invariant circles born at Neimarck-Sacker bifurcations. They are destroyed either in heteroclinic tangencies (see e.g. [2]), or in a more complicated bifurcation that seems to involve loss of invertibility and possibly hyperbolicity in a collision of the circle with its preimage at the critical point. See [14] for research in this direction.

Another global aspect of the dynamics is the interaction of the 1:3 resonance with other resonances. Indeed, near the 1:3 resonance there is a dense set of parameter points on the main cardioid that correspond to higher resonances. Each of these resonances gives rise to an Arnol'd tongue (for $\alpha \neq 1$), with the tip on the main cardioid, compare Figures 1 and 2. The tongue is pointing inwards or outwards, depending on the sign of $\alpha - 1$, cf. [4,

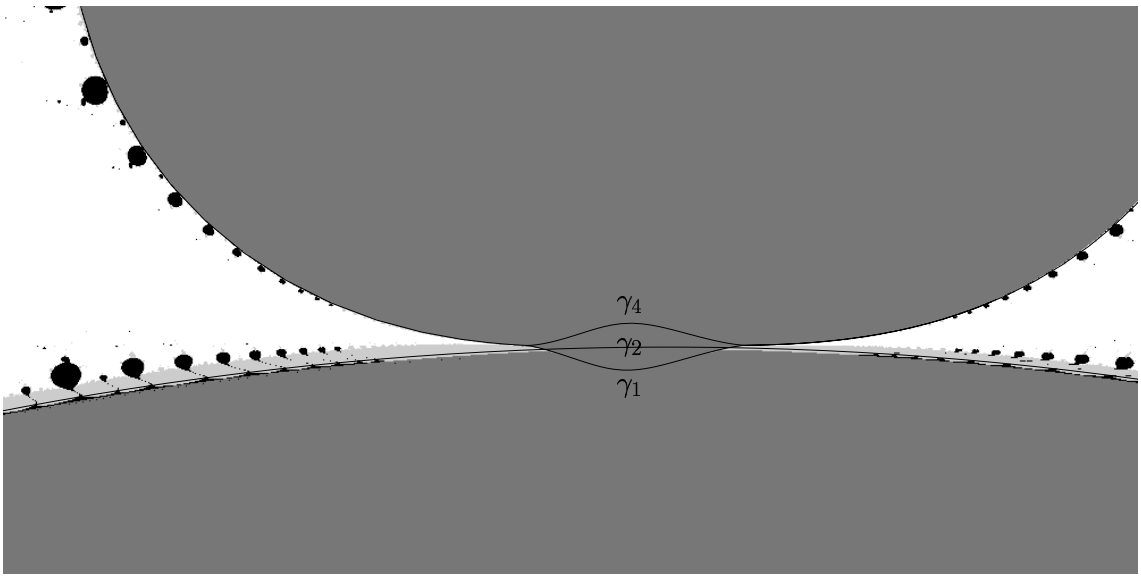

FIGURE 1. The fate of the critical point, in a part of the c-plane near the 1:3 resonance, for $\alpha = 1.1$. In the white region it escapes to infinity, in the dark grey region it converges to a period 1 or 3 orbit, and in the black regions to a periodic orbit of period at least 4 and at most 46. In the light grey regions, the motion is "undetermined", which can indicate an invariant circle or an attracting orbit of high period, or chaotic motion. The lines indicate curves of saddle-node (for γ_1 and γ_4) or Neimarck-Sacker bifurcations (for γ_2). See Figure 3 for more details.

Section 4]. Outside the Arnol'd tongues, the main cardioid corresponds to a Neimarck-Sacker bifurcation. The invariant circle created in this bifurcation undergoes a saddle-node bifurcation on the boundaries of an Arnol'd tongue, changing it into a ring of saddles and nodes, connected by invariant manifolds.

To study the dynamics more thoroughly, we propose to construct a vector field that qualitatively describes the essential dynamics. Following Takens [26], we show the existence of a vector field such that its time 1 flow, composed with a rotation over $2\pi/3$, is a small perturbation of the map $f_{\alpha,c}$. The vector field is obtained by a normal form computation, and the perturbation can be made arbitrarily small in a neighborhood of the 1:3 resonance point in phase-parameter space. In particular, the vector field will capture all local bifurcations. The present paper presents and analyzes such a vector field in the holomorphic case $\alpha = 1$, showing that its dynamics corresponds nicely to the dynamics of the map. We intend to pursue this matter further in future research.

1.2. **Overview.** In the next section we recall well known theory on the quadratic map, and fix some notation. Sections 3 and 4 deal with the bifurcation diagram for $\alpha > 1$ and $\alpha < 1$, respectively. Arnol'd tongues are discussed in Section 5, while Section 6 presents a vector field model for the holomorphic case $\alpha = 1$. The normal form theory used to obtain this model is explained in Appendix A and B. Appendix C gives some background information on external rays.

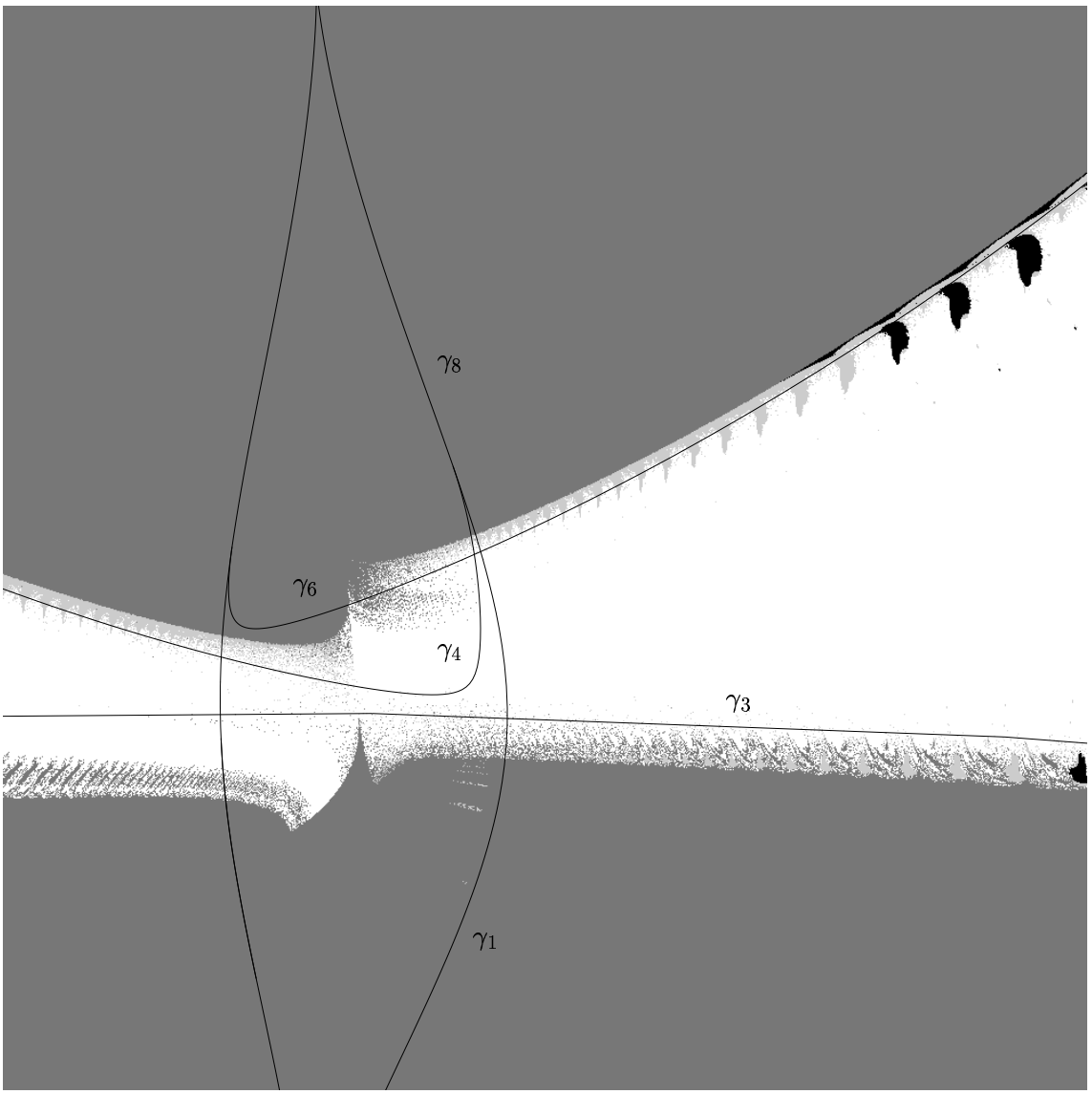

FIGURE 2. The fate of the critical point, in a part of the c-plane near the 1:3 resonance, for $\alpha = 0.9$. The color coding is the same as in Figure 1. The curves are saddle-node (for γ_1, γ_8) or Neimarck-Sacker bifurcations (for $\gamma_3, \gamma_4, \gamma_6$), cf. Figure 8.

1.3. **Acknowledgements:** We would like to thank H. W. Broer, B. Peckham, F. Takens and F. Wagener for useful discussions and R. Vitolo for his assistance with computer software. We are also grateful for the careful reading and suggestions of the referee.

2. PRELIMINARIES

The family $f_{\alpha,c}(z) = |z|^{2\alpha-2}z^2 + c$ has been studied by more people than the literature suggests. Local connectivity of $\mathcal{M}_\alpha$ and the construction of external rays (especially in

parameter space) is an intriguing and also hard problem. It should be noted that $f_{\alpha,c}$ is a plausible complexification of the unimodal interval map $x \mapsto |x|^{2\alpha} + c$. One motivation for external rays is therefore that it can shed light on the monotonicity problem of topological entropy for $x \mapsto |x|^{2\alpha} + c$, cf. [12], which is still open for $\alpha \notin \mathbb{N}$.

Another topic has been the structure of the Julia set for c close to 0. For $\alpha \approx 1$, J_c is a topological circle which carries hyperbolic dynamics conjugate to the angle doubling map. Depending on the relative positions of $\alpha - 1$ and $|c|$, this circle is smooth (and normally hyperbolic) [4] or non-rectifiable with Hausdorff dimension > 1, [17, 25].

Let us starts describing the *main cardioid* as function of α. Depending on the choice of coordinates, we can write $f_{\alpha,c}$ as

$$\begin{aligned} f_{\alpha,c}(z) &= |z|^{2\alpha-2}z^2 + c \\ &= r^{2\alpha}e^{2i\varphi} + c \\ &= (x^2+y^2)^{\alpha-1}(x^2-y^2) + \mathrm{Re}\ c \ + \ (2(x^2+y^2)^{\alpha-1}xy + \mathrm{Im}\ c)\ i, \end{aligned}$$

where $z = re^{i\varphi} = x + iy$. Using polar coordinates, one easily computes

$$Df = 2r^{2\alpha-1}\begin{pmatrix} \alpha\cos 2\varphi\cos\varphi + \sin 2\varphi\sin\varphi & \alpha\cos 2\varphi\sin\varphi - \sin 2\varphi\cos\varphi \\ \alpha\sin 2\varphi\cos\varphi - \cos 2\varphi\sin\varphi & \alpha\sin 2\varphi\sin\varphi + \cos 2\varphi\cos\varphi \end{pmatrix}.$$

This gives for the trace and determinant

$$\mathrm{tr}\ Df = 2r^{2\alpha-1}(\alpha+1)\cos\varphi,\ \det Df = 4\alpha r^{2(2\alpha-1)}.$$

The curve in phase space with $\det Df = 1$ is a circle with radius $r_0 = (2\sqrt{\alpha})^{-1/(2\alpha-1)}$. The boundary of the *main cardioid* is the curve in parameter space such that one of the fixed points, we call it the central fixed point p, has $\det Df(p) = 1$. This means that p is non-hyperbolic, undergoing a Neimarck-Sacker or more complicated bifurcation, or p is a hyperbolic saddle, whose eigenvalues happen to multiply to 1. To compute it, we need to solve $p = r_0e^{i\varphi} = f(p) = r_0^{2\alpha}e^{2i\varphi} + c$, which gives

$$c_0 := c = \alpha^{-\frac{1}{2}}2^{-\frac{1}{2\alpha-1}}e^{i\varphi} - \alpha^{-\alpha}2^{-\frac{2\alpha}{2\alpha-1}}e^{2i\varphi}. \tag{2}$$

This describes a limaçon-shaped curve. For $\alpha < 1$ it has a small inner loop near $c = \frac{1}{4}$, for $\alpha = 1$ we have the well-known cardioid, and for $\alpha > 1$ the cusp in the cardioid flattens to a smooth curve. The multiplier μ of $p = r_0e^{i\varphi}$ is $e^{i\vartheta}$, where $2\cos\vartheta = \mathrm{tr}\ Df(p) = 2r_0^{2\alpha-1}(\alpha+1)\cos\varphi$, so

$$\cos\vartheta = \frac{\alpha+1}{2\sqrt{\alpha}}\cos\varphi. \tag{3}$$

The conformality at $\alpha = 1$ prevents several features to occur which are present for $\alpha \neq 1$. Examples are saddle points, normally hyperbolic invariant cycles conjugate to rotations (due to Schwarz' lemma) and hence Neimarck-Sacker bifurcations, and the coexistence of several periodic attractors. Let us define the filled-in Julia set $K_c = \{z \in \mathbb{C} \mid f^n(z) \not\to \infty\}$ and $A(\infty) = \mathbb{C} \setminus K_c$ is the basin of infinity. Note that officially, the Julia set J_c is defined as the set of points z such that $f_{\alpha,c}^n : U \to \overline{\mathbb{C}},\ n \in \mathbb{N}$ is not an equicontinuous family on any neighborhood U of z. Since Montel's Theorem no longer holds for $\alpha \neq 1$, one cannot conclude that J_c is the common boundary of K_c and $A(\infty)$. When discussing the global behaviour of f, we will be interested in $\partial A(\infty) = \partial K_c$ rather than in J_c, and call this set the Julia set (slightly abusing terminology).

As in the conformal case, K_c is connected and full, i.e., $A(\infty)$ consists of a single component, if and only if the critical point has a bounded orbit. The argument is based on a straightforward adaptation of the construction of external rays (included in Appendix C) and roughly suggests the global shape of the Julia set. It indicates that $\partial A(\infty)$ is a topological factor of a circle (Caratheodory loop), where each $z \in \partial A(\infty)$ arises from identifying a bounded number of points of the circle. The action $f_{\alpha_c}|\partial A(\infty)$ and the angle doubling map $z \mapsto z^2$ on the unit circle have a common factor (we explain this in more detail in Appendix C), and as a result, it has at least the complexity of a factor of the full two-shift. Therefore, for generic α, $\partial A(\infty)$ is expected to contain $2^n - 1$ points of period n for co-finitely many n. For example, we always expect to find a fixed point on $\partial A(\infty)$ with *external angle* 0, which we call p' in this paper. The other fixed point, called p, plays a role in the 1:3 bifurcation discussed in this paper. In the conformal version of this bifurcation, one period 3 orbit collapses to this fixed point.

3. The 1:3 bifurcation diagram, for $\alpha > 1$.

In this section we give a global description of the bifurcation diagram corresponding to the creation of the period 3 sink that occurs at the top side of the locus of existence of an attracting fixed point. In the conformal case ($\alpha = 1$), this period 3 sink emerges in a Leau-Fatou-bifurcation at the parameter value $c = \frac{1}{2}e^{i\varphi} - \frac{1}{4}e^{2i\varphi}$, for $\varphi = \frac{2\pi}{3}$, see e.g. [9]. For $\alpha > 1$, the bifurcation diagram is as displayed in Figure 3, which shows the particular case $\alpha = 1.1$. It consists of seven regions (1 - 7) separated by curves γ_i, $i = 1, \dots 8$ (curve γ_8 is too small to be seen on this scale). All curves are computed numerically by AUTO [10, 11], except for γ_3, γ_5, γ_7 and γ_8, whose existence is conjectured for reasons explained below. In fact, we conjecture that these four curves are generically narrow regions rather than curves. Phase portraits are shown for relevant regions in the bifurcation diagram. In order to focus on the important aspects of the dynamics we will omit phase portraits of small regions with trivial or otherwise uninteresting dynamics, and of regions with dynamics very similar to a displayed phase portrait of another region. The dynamics in the two unlabeled regions on the left is similar to that in the corresponding regions 6 and 7 on the right. Therefore these two are omitted from the analysis. The region between γ_5 and γ_7 is conjectured to be very narrow. In this region the dynamics near the central fixed point is trivial, simply consisting of a repelling fixed point surrounded by a period three repeller, and is therefore not analyzed.

There are five codimension two local bifurcation points in this part of phase-parameter space: a 1:3 resonance point (not marked), two cusp points, indicated by **C**, and two Bogdanov-Takens points (**BT**) in the context of maps, compare [5]. At the 1:3 resonance point, a curve of Neimarck-Sacker bifurcations is tangent to a narrow region of heteroclinic tangle, cf. [19]. Two curves of saddle-sink bifurcations intersect tangentially at the cusp points. A Bogdanov-Takens point arises when a curve of Neimarck-Sacker bifurcations and a narrow region of heteroclinic tangle end tangentially at a curve of saddle-node bifurcations, and the node changes stability at the bifurcation point. The cusp and Bogdanov-Takens points are extremely close together, and their separation becomes visible only after a huge magnification of the relevant parameter region, see Figure 4. In this figure one can also see the location of γ_8. We do not show phase portraits for some very small regions near the Bogdanov-Takens point, as this bifurcation is well understood.

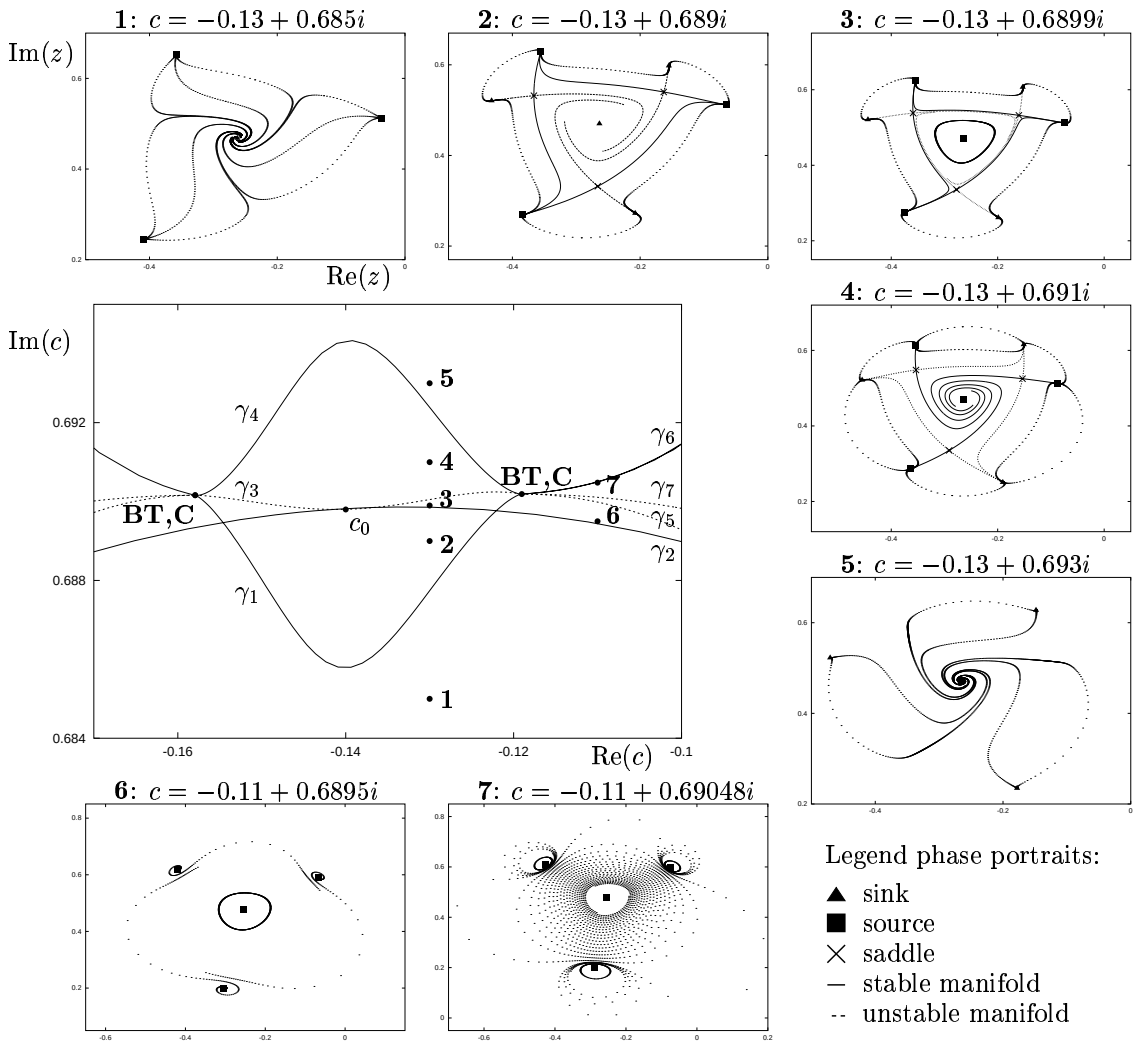

FIGURE 3. Bifurcation diagram and phase portraits of the unimodal map near the 1:3 resonance point, for $\alpha = 1.1$. Phase portraits are located at the indicated parameter points. In each phase portrait, p is the organizing fixed point (but not labeled in order not to clod up the picture) whereas p' is far outside the picture. The organizing center of the bifurcation diagram is the 1:3 resonance point c_0, see (2). The dynamics is explained in Section 3. The solid curves in the bifurcation diagram are computed by a continuation method, the dashed ones are conjectured.

Let us describe the dynamics in each of the regions 1 – 7 and at the transition curves. For numerically computed phase portraits in each of the regions we again refer to Figure 3. In these diagrams, dots correspond to orbit points, while solid curves indicate stable manifolds of a saddle point, and dashed curves indicate unstable manifolds. We remark that these manifolds are well-defined locally, that is, not beyond the critical point. Due to the 2-to-1 covering, the stable manifold has infinitely many branches, and we select the branch connected to the saddle point, cf. [13, 14, 24]. The phase portraits are computed by DsTool [3, 18].

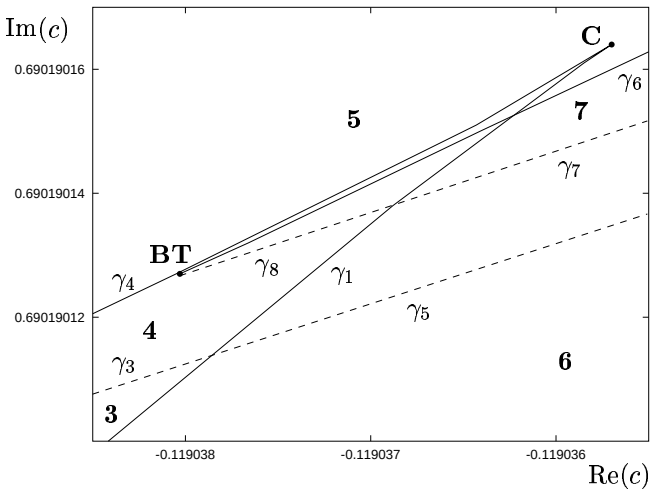

FIGURE 4. Zoom-in of the bifurcation diagram for $\alpha = 1.1$ on the rightmost cusp and Bogdanov-Takens point, cf. Figure 3.

Region 1: The map f has two fixed points, one of which, p, is attracting, and it attracts the critical point. Note that unlike the holomorphic case, coexistence of several attractors is now possible. The common boundary $\partial A(p) = \partial A(\infty)$ of the basins of p and ∞ contains the other fixed point p', as well as two period 3 orbits. The fixed point p' is hyperbolic repelling, and it belongs to $\partial A(\infty)$. We expect that all periodic points other than the fixed point p belong to $\partial A(\infty) = \partial A(p)$. The numerical evidence for these last observations (concerning $\partial A(\infty)$) apply to the local parameter range discussed in this section. The equality $\partial A(p) = \partial A(\infty)$ cannot hold globally in the main cardioid close to its boundary, see e.g. [4].

Region 2: Coexistence of the attracting fixed point p and a period 3 sink, attracting the critical point. The fixed point p is surrounded by a "triangular" ring of period 3 saddle-source connections. The preimages of the immediate basins of the period 3 sink (the ears and body of the rabbit) and of p have a comparable intricate pattern as is known from Douady's rabbit. As a result, the fixed point p' does not belong to the boundary of any of these preimages, but it still belongs to $\partial A(\infty)$. The period 3 sources in the saddle-source connection belong to $\partial A(\infty)$ as well.

Curve γ_1: Traversing from region 1 into region 2 or from region 6 into region 3, a saddle-sink bifurcation occurs creating a period 3 sink and saddle out of nothing.

Region 3: The period 3 sinks (attracting the critical point), saddles and sources of region 2 coexist with the fixed point p. This point is repelling and surrounded by an attracting invariant circle Γ, which either carries an irrational rotation with rotation number close to $\frac{1}{3}$, or is at resonance (and then it is a ring of saddle-sink connections). A further discussion of corresponding Arnol'd tongues is given in Section 5.

We remark that if the circle Γ is at resonance with another period than 3, then this does not create conflicts in the geometry: The inward unstable manifolds of the 3 saddles intersect the outward stable manifolds of the saddles on the curve of saddle-sink connections Γ, but these intersections do not lead to heteroclinic

behaviour. In Figure 5 we illustrate these intersections schematically for the case that Γ contains only two saddles. The critical point is attracted to the period 3 sink, hence not to Γ.

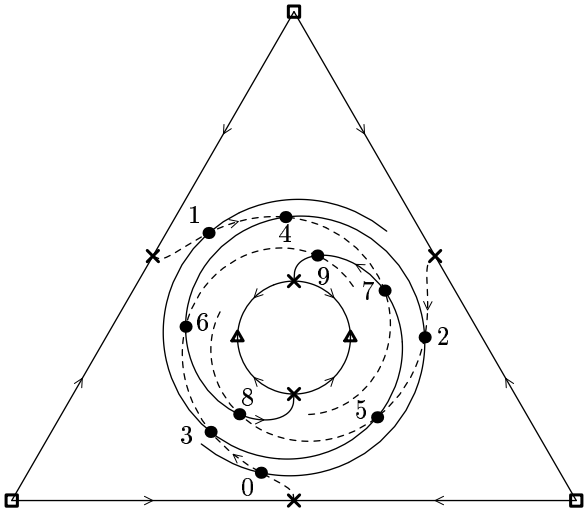

FIGURE 5. Sketch of the Neimarck-Sacker circle in resonance (center), surrounded by a period three saddle orbit, for a parameter point in region 3 of figure 3. Solid lines indicate stable manifolds, dashed lines unstable ones. The sketch demonstrates that there is no obstruction against transversal intersections of the invariant manifolds of the period three saddle and those of the saddle orbit on the circle. The points $0 - 9$ are iterates of a sample intersection point.

Curve γ_2: Traversing γ_2 from region 2 into region 3, the fixed point p undergoes a Neimarck-Sacker bifurcation, generating an invariant circle Γ and itself becoming repelling. The Neimarck-Sacker bifurcation can be at resonance; this indicates the tip of an Arnol'd tongue, see Section 5.

Traversing γ_2 from region 2 into region 4, one passes through the organizing center c_0 with polar coordinates $r_0 = (4\alpha)^{-1/(4\alpha-2)}$ and $\cos\varphi_0 = \frac{1+\alpha}{2\sqrt{\alpha}} \cos\frac{2\pi}{3}$, see (3). For fixed $\alpha > 1$, the map f_c seems to unfold generically at this codimension 2 bifurcation, see e.g. Kuznetsov [19]. In particular, the curve γ_2 and pinched sickle shape region γ_3 have quadratic tangency at c_0.

Between region 1 and region 6, γ_2 is a curve of Neimarck-Sacker bifurcations, possibly at resonance. In contrast to the conformal case, it does not belong to the boundary of the Mandelbrot set, see below for more details.

Region 4: A period 3 sink is part of a ring of saddle-sink connections, surrounding the fixed point p which is repelling. The critical orbit converges to the period 3 sinks. One part of the stable manifold of each of the period 3 saddles connects with a period 3 source, which belongs to $\partial A(\infty)$.

"Curve" γ_3: The Neimarck-Sacker circle Γ clashes with the ring of saddle-source connections, destroying both and leaving a ring of period 3 saddle-sink connections. Most likely, this clash is not the tangential collision of the two circular curves (known from the continuous time version of the 1:3 resonant Hopf bifurcation, see

e.g. [19]), but it involves a heteroclinic bifurcation, in which the unstable manifold of one period 3 saddle intersects the stable manifold of the neighboring period 3 saddle, creating a heteroclinic tangle with the corresponding chaotic dynamics. Theoretically, these heteroclinic intersections occur in an exponentially narrow (in terms of distance to the organizing center) region, bounded by curves of heteroclinic tangencies. Since the existence of region γ_3 presupposes the existence of a saddle and a Neimarck-Sacker circle, γ_3 lies above γ_2 and between γ_1 and γ_4. We do not know where exactly γ_3 ends; Numerical evidence suggests that its endpoints are very close to the cusps.

Region 5: No period 3 saddles and sources exist close to the repelling fixed point p. The period 3 sinks attract the critical orbit. Their immediate basins have the repelling fixed point p as common boundary point. At the same time $p \in \partial A(\infty)$.

Curve γ_4: Traversing γ_4 from region 4 into region 5 between the two Bogdanov-Takens points a saddle-source bifurcation occurs in which the period 3 saddles and period 3 sources merge and disappear. If the curve is traversed between a Bogdanov-Takens point and the nearby cusp point, then the bifurcation is of saddle sink type.

Region 6: No period 3 sink exists. The fixed point p is repelling and surrounded by an attracting invariant circle Γ, which either carries an irrational rotation number, or is at resonance (and hence is a ring of saddle-sink connections). Region 6 therefore contains infinitely many Arnol'd tongues, see the schematic Figure 12. The circle Γ attracts the critical point, and hence the curve γ_2 does not bound the locus of connectivity of the complement of $A(\infty)$.

Region 7: The point p is repelling and a repelling period three orbit is surrounded by an attracting invariant 3-circle, which grows when moving down in region 7.

"Curve" γ_5: Moving from region 6 upwards through γ_5, we conjecture that the curve Γ is destroyed shortly before it collides with $\partial A(\infty)$. Indeed, when moving upwards within region 6, Γ increases in size, and approaches the critical point. Here Γ looses its smoothness, and conjecturally also its invertibility, see Figure 6. We conjecture that the resulting "chaotic" set eventually collides with $\partial A(\infty)$. At that time the critical point could theoretically escape to ∞, and render $A(\infty)^c$ disconnected (with infinitely many connected components).

Figure 7 shows in more detail the loss of smoothness, and conjecturally quasiperiodic motion, of Γ; it shows features similar to those discussed in [6], which are thought to be caused by heteroclinic tangencies of saddles on the invariant "circle" in resonance. The "chaotic" set is still attracting. To our best knowledge, the transition from γ_3 to γ_5 is an open problem.

Curve γ_6: When entering region 5 from region 7 one passes through γ_6, which is a curve of Neimarck-Sacker bifurcations (possibly at resonance), at which a triple of invariant attracting period 3 curves merges into a period 3 orbit, changing this orbit from repelling to attracting.

"Curve" γ_7: Moving down from region 7 through γ_7, we conjecture that the 3-circle of region 7 is destroyed in a collision with the critical point, similar to the bifurcation on γ_5.

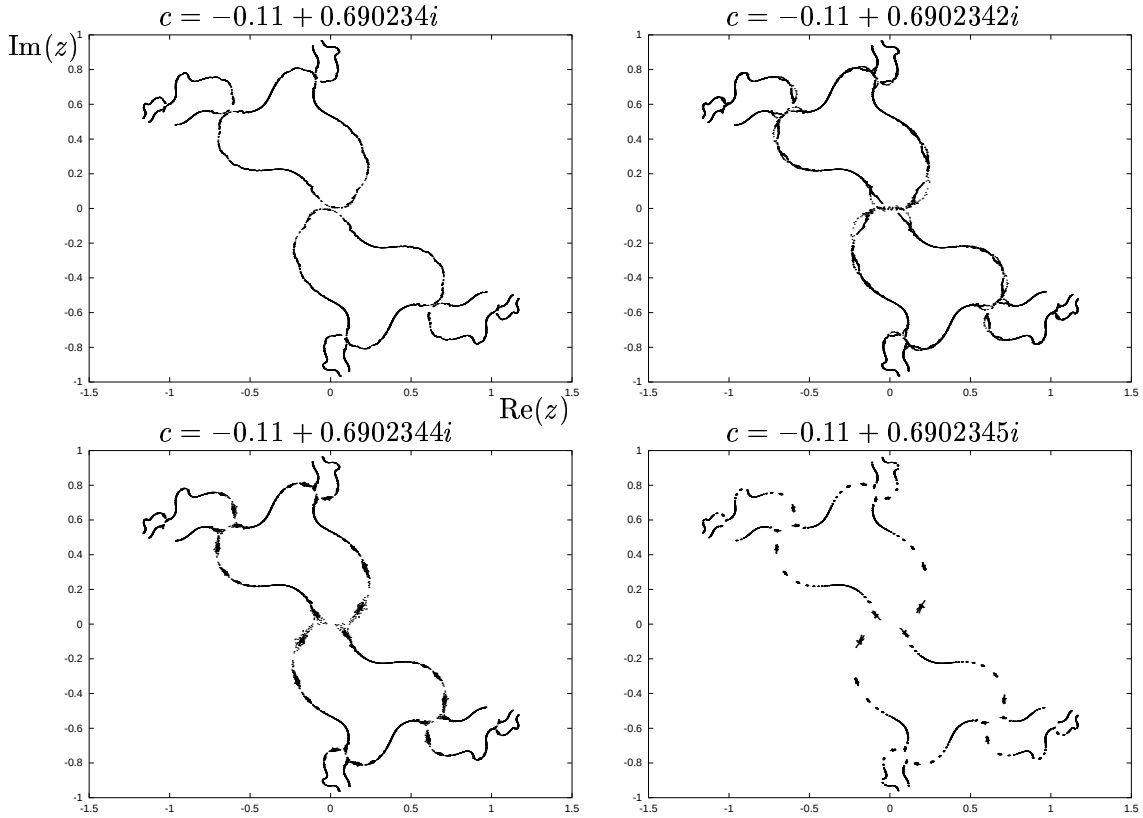

FIGURE 6. The Neimarck-Sacker circle Γ for $\alpha = 1.1$ and (a finite number of) its preimages under f, at the indicated parameter points, near γ_5. In the top left diagram the Neimarck-Sacker circle – the big closed curve just above the critical point – seems to be intact, that is, the parameter point is below γ_5. The top right diagram is very close to the merging point, while in the bottom diagrams the curve has merged with its preimages. The dynamics on the resulting curve is angle doubling.

"Curve" γ_8: (See Figure 4.) This curve actually is a region which is exponentially narrow with respect to the distance to the Bogdanov-Takens point, corresponding to a heteroclinic tangle in which the 3-circle created in the Neimarck-Sacker bifurcation at γ_6 is destroyed. This bifurcation is similar to the one on γ_3.

The disappearance of the Neimarck-Sacker circle in a clash with its preimages and the Julia set has an analogue in the holomorphic case $\alpha = 1$. In this case, if c is a parameter point on the boundary of the main cardioid satisfying a Diophantine condition, then the map $f_{1,c}$ has a Siegel disk, consisting of invariant closed curves that wind around the fixed point p, and the boundary of the Siegel disk contains the critical point, cf. [15]. Let us consider a curve in the parameter plane passing transversally through the main cardioid at such a Diophantine point. In the resulting three dimensional combined phase-parameter space, the Siegel disk separates two regions where the fixed point p is attracting or repelling, respectively. We conjecture that this separation persists under the nonanalytic

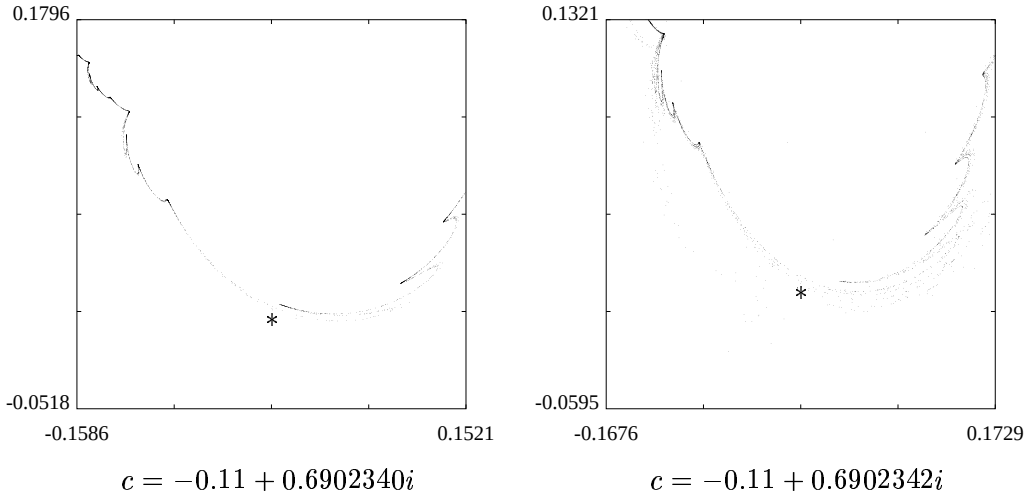

FIGURE 7. Zoom-in in Figure 6 (i.e., $\alpha = 1.1$) near the critical point, indicated by $*$, shows the destruction of the attracting Neimarck-Sacker circle Γ as it approaches the critical point.

perturbation, resulting in a *skewed* Siegel disk, that is, with a single invariant circle for every parameter point on the curve on one side of the main cardioid.

4. The 1:3 bifurcation diagram, for $\alpha < 1$.

In this section we analyse the bifurcations of $f_{\alpha,c}$ for $\alpha < 1$ but close to 1, near the 1:3 resonance point. A bifurcation diagram for $\alpha = 0.9$ is displayed in Figure 8. All bifurcation curves are computed numerically by AUTO [10, 11], except for γ_2, γ_5, γ_7 and γ_9. The existence of these four follows from the dynamical properties of the map. In fact, we expect γ_2, γ_5, γ_7 and γ_9 to correspond to narrow regions rather than curves.

The bifurcation diagram is organized by the 1:3 resonance point and four other codimension two points. Based on our numerical explorations we classify two of them as cusps, and the other two as Bogdanov-Takens points. The coding of cusps and Bogdanov-Takens points is as in Section 3.

The nine curves γ_i, $i = 1, \ldots, 9$ divide the parameter domain in 12 regions. We describe the dynamics in these regions, and the transitions from one region to another, one by one. We note that there are four small regions in the parameter plane, near the right Bogdanov-Takens point, where we do not show a phase portrait. The reason is that the dynamics in these regions is the same as in regions 4, 5, 6 and 7, except that the order of two unrelated Neimarck-Sacker bifurcations is reversed. Moreover, the dynamics of regions 10, 11 and 12 is similar to the dynamics in the corresponding regions to the right of the central part of the bifurcation diagram, and hence the latter trio will not be discussed. Finally, there is a very small unlabeled region bounded by γ_1, γ_2 and γ_9, that will be discussed together with the curve γ_9, see below.

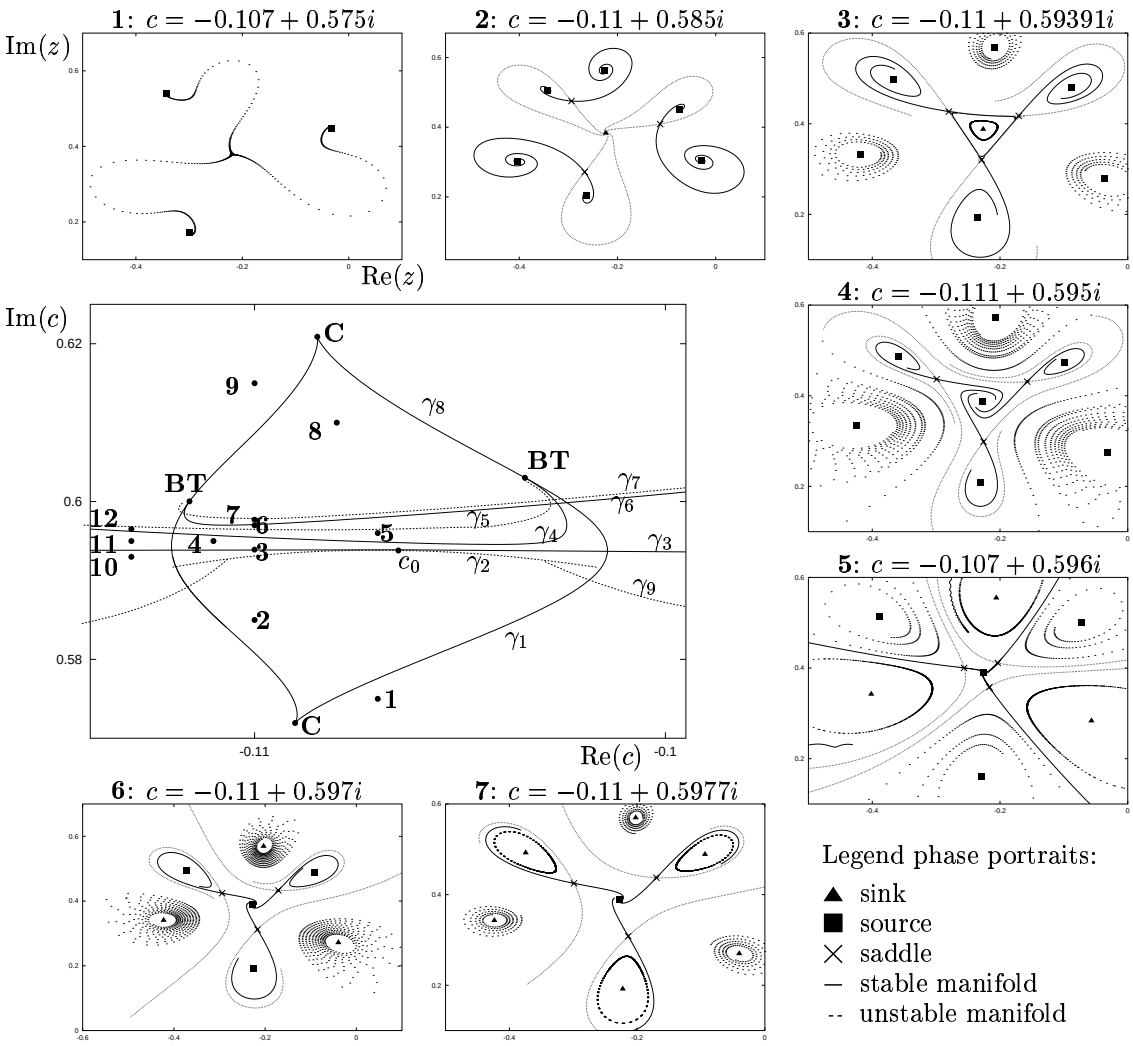

FIGURE 8. Bifurcation diagram and phase portraits of the unimodal map near the 1:3 resonance point, for $\alpha = 0.9$. Phase portraits are located at the indicated parameter points. The role of p, p' and c_0 is as in Figure 3. The dynamics is explained in Section 4. The solid curves in the bifurcation diagram are computed by a continuation method, the dashed ones are conjectured. Continued in the next figure.

Figures 8 and 9 show a phase portrait for each region, computed by DsTool [3, 18]. In the phase portraits, dots correspond to orbits, while solid and dashed curves correspond to stable and unstable manifolds, respectively. We note that at each parameter point there exists a repelling fixed point, p' and a repelling period three orbit, that are not involved in any of the bifurcations we describe, and are in fact located on the boundary of $A(\infty)$. Consequently, these periodic points are ignored in the sequel.

Region 1: The map has an attracting fixed point (attracting the critical point) and a repelling period three orbit.

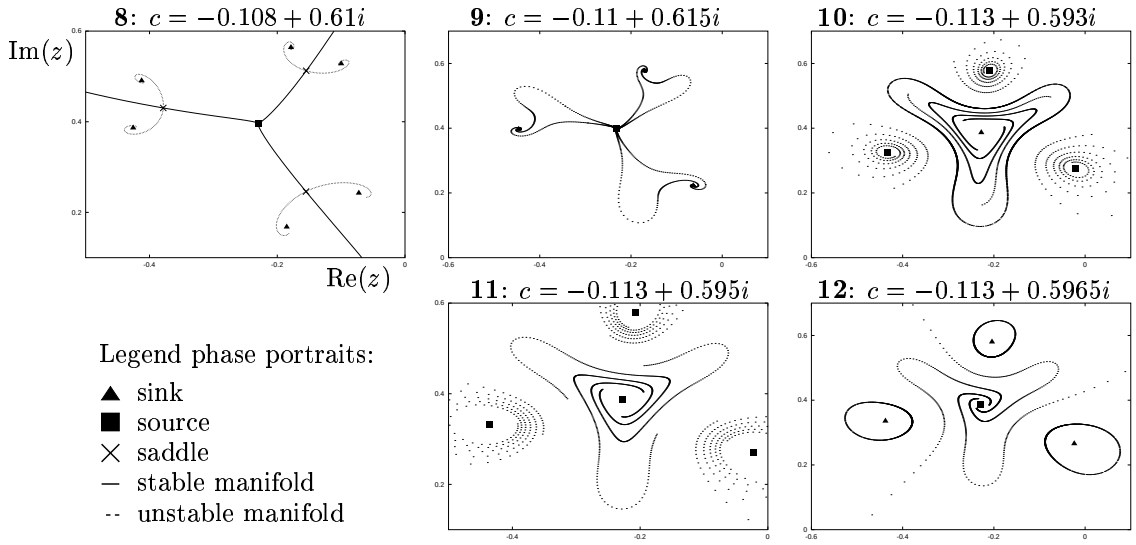

FIGURE 9. Phase portraits of the unimodal map near the 1:3 resonance point, for $\alpha = 0.9$. Continued from the previous figure.

Region 2: Apart from the attracting fixed point there are two repelling period three orbits and one period three saddle. The unstable manifolds of each saddle point (both) go to the fixed point, while the stable manifolds converge to two period three points.

Curve γ_1: This is a curve of period three saddle-source bifurcations, consisting of two smooth branches, joining at the lower cusp point and ending at the Bogdanov-Takens points. Going from region 1 to region 2, a period three saddle and source are created. The same bifurcation occurs on γ_1 between regions 10 and 3, 10 and 2, 11 and 4, 12 and 5, or 9 and 6. On the left branch of γ_1 the saddle orbit collides with one of the period three repellers present in region 2, while on the right branch it collides with the other, which necessitates the cusp in between.

Region 3: The attracting fixed point is surrounded by a repelling invariant circle. This circle either has irrational rotation number or it is at resonance, in which case the dynamics consists of a ring of saddle-source connections. Further there are two repelling and one saddle period three orbit. The stable manifolds of the saddles converge to the invariant circle and one of the period three repellers, while the unstable manifolds diverge. The critical orbit diverges to ∞, rendering $\partial A(\infty)$ disconnected.

"Curve" γ_2: Between regions 2 and 3 a heteroclinic tangle corresponding to the period three saddle exists in a narrow domain indicated by the curve γ_2. On the boundaries of the domain the invariant manifolds of the saddles are tangent, while they intersect transversally in the interior. By this mechanism an invariant circle is created when traversing γ_2 into region 3. The region indicated by γ_2 will be pinched at and tangent to the 1:3 resonance point on γ_3.

Region 4: A repelling fixed point is surrounded by a period three saddle orbit and two period three repellers. The unstable manifolds of the saddles escape to ∞, while the stable manifolds go to the fixed point or to one triple of the period 3

repellers. When moving from left to right in region 4, the latter stable manifolds switch from one set of repellers to the other. We call this process a *stable manifold switch.*

The critical orbit tends also to ∞, except when 0 lies on the stable manifold of the period 3 saddle orbit. This indeed happens, as numerical evidence shows, in a more or less vertical curve, near $Re(c) = -0.107$, that crosses regions $4, \ldots, 8$.

Curve γ_3: Traversing γ_3 from region 3 into region 4 or from region 10 into 11, the invariant circle is destroyed in a Neimarck-Sacker bifurcation at the fixed point. Going directly from region 2 to region 4 through the 1:3 resonance point, the period three saddle points pass through the fixed point, changing the stability type of the latter.

Region 5: The repelling fixed point is encircled by 3 period three orbits, one repelling, one attracting and one of saddle type. The attracting period three points are surrounded by repelling invariant 3-circles. The unstable manifolds of the saddles diverge, while the stable ones go to the repelling fixed and, depending on whether c belongs to the left or right side of region 5, to the period 3 repellers or the period 3 invariant circles. The critical orbit diverges to ∞, except when 0 belongs to the stable manifold of the period 3 saddle orbit.

Curve γ_4: Crossing this curve from region 4 into 5 or from region 11 into 12, a Neimarck-Sacker bifurcation occurs at one of the (in the latter case, the only) period three repellers.

Region 6: There is one repelling, one attracting and one saddle period three orbit, as well as a repelling fixed point, but the period 3 circle from region 5 no longer exists. The critical point is attracted to the period 3 sink, except when it belongs to the stable manifold of the period 3 saddle orbit.

"Curve" γ_5: Going from region 5 to 6, or from 12 to 9, the period 3 circle is destroyed. Based on numerical results and bifurcation theory for Bogdanov-Takens points of maps, we conjecture that near the (right hand) Bogdanov-Takens point there exists a region where the invariant manifolds of the three period three saddles form a heteroclinic tangle. This region, indicated by γ_5, is tangent to the curve of saddle-nodes at the Bogdanov-Takens point, and is exponentially narrow with respect to the distance to this point. On the boundaries of this region the manifolds are tangent. When approaching γ_5 from region 5, the 3-circle grows and collides with the stable manifolds of the saddles. Generically one expects the invariant circle to loose differentiability before being destroyed, cf. [5].

We conjecture that further away from the Bogdanov-Takens point (e.g. left from the stable manifold switch, when the stable manifold wraps around the other period 3 source), the 3-circles are destroyed when they come close to the critical point, see Figure 10.

The bifurcations, and a collision with $\partial A(\infty)$ could be comparable to the scenario proposed for γ_5 in Figure 4 for the case $\alpha = 1.1$. However, we observe that the case $\alpha < 1$ has an additional complication (compared to $\alpha > 1$). Indeed, an orbit passing through the critical point has two Lyapunov exponents equal to $-\infty$, whereas an orbit on the repelling Neimarck-Sacker circle has one positive and one zero exponent. This implies that the positive exponent has to pass through zero before the invariant circle clashes with the critical point, probably leading to a loss of hyperbolicity (of the invariant circle).

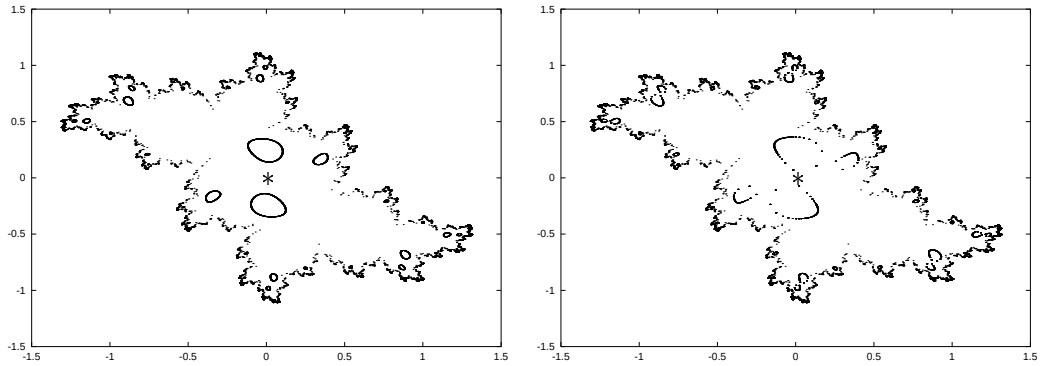

FIGURE 10. Destruction on γ_5 of repelling period 3 Neimarck-Sacker circles close to the critical point, for $\alpha = 0.9$. In addition to the (destroyed) 3-circle directly above the critical point (marked $*$), some preimages under $f^3_{\alpha,c}$ of the Neimarck-Sacker circle are shown. The other two invariant 3-circles are not displayed for clarity. The left diagram is situated below γ_5. In the right diagram it seems that the 3-circle is broken. We conjecture it lost its hyperbolicity. At $c = -0.11+0.5964$ (not displayed) the circle has disappeared completely.

Region 7: There is a repelling fixed point, and two attracting and one saddle period 3 orbit. One of the attracting orbits is surrounded by a repelling 3-circle. The critical orbit converges to the period 3 sinks without invariant circles, except when it lies on the stable manifold of the period 3 saddle orbit.

Curve γ_6: Going from region 6 to region 7, the (unique) repelling period 3 orbit undergoes a Neimarck-Sacker bifurcation, creating a repelling 3-circle and stabilizing the periodic orbit.

Region 8: A repelling fixed point is accompanied by two period 3 attractors, as well as a period three saddle orbit. The critical orbit is attracted to one of the period 3 attractors, except at the stable manifold switch. No repelling 3-circle exists.

"Curve" γ_7: Traversing from region 7 into region 8, the 3-circle created at γ_6 is destroyed. Near the (left-hand) Bogdanov-Takens point this happens in a heteroclinic tangle. The dynamics is very much like in the case of γ_5, including the "collision" of the period 3 Neimarck-Sacker circles to the right of the stable manifold switch.

Region 9: In this region, a repelling fixed point coexists with an attracting period 3 orbit, which attracts the critical orbit.

Curve γ_8: Between regions 8 and 9 a saddle-sink bifurcation occurs, destroying one period three saddle and one of the period three sink orbits. The cusp point can be explained in the same way as the one on γ_1.

Region 10: An attracting fixed point is surrounded by a repelling invariant circle and a repelling period three orbit. The critical orbit escapes to ∞, the set $\partial A(\infty)$ is disconnected and contains the invariant circle and all its preimages.

"Curve" γ_9: Crossing "curve" or rather narrow region γ_9 from region 10 into region 1, we conjecture that an invariant circle approaches the critical point and disintegrates, cf. Figure 6 with reversed stability. The remainder of the circle collides with $\partial A(\infty)$.

Traversing region 10 into region 2, this circle surrounds the triangle of period 3 saddles, while it is inside this triangle when we go from region 10 to region 3. Going from region 3 to 2, one of the stable manifolds of the period three saddle crosses both unstable manifolds, see Figure 11 (cf. also [16]). In the first crossing the invariant circle inside the triangle is destroyed, while the last crossing corresponds to the birth of the circle outside the triangle.

Region 11: A repelling fixed point coexists with a repelling period three orbit. The critical orbit diverges. There is no invariant circle.

Region 12: In this region the fixed point is repelling, and there is an attracting period three orbit encircled by a repelling invariant 3-circle. The critical orbit diverges.

5. Arnol'd tongues

For the conformal map $f_{1,c} : z \mapsto z^2 + c$, the parameter regions for which $f_{1,c}$ has a hyperbolically attracting periodic orbit are known as *hyperbolic components*. These are topological disks, containing a *center* at which parameter the critical point itself is a superattracting periodic point, cf. [9, Theorem VIII 2.1] or [20]. From the main cardioid (the hyperbolic component of period 1), infinitely many hyperbolic components emerge, namely at those parameters c for which the multiplier of the central fixed point is a root of unity. All these bifurcations are so-called Leau-Fatou-bifurcations.

For the nonconformal case, the central fixed point p looses stability in a Neimarck-Sacker bifurcation, and Arnol'd tongues in the parameter space that indicate that the Neimarck-Sacker circle is in resonance can be viewed as the continuation of the hyperbolic components of the Mandelbrot set $\mathcal{M}_1$ directly attached to the main cardioid. A simple counting argument gives, for generic α, that these Arnol'd tongues too should contain a *center*, i.e., a parameter for which the critical point 0 is periodic with the period of the resonance.

Lemma 1. *The family $f_{\alpha,c}(z) = r^{2\alpha}e^{2i\varphi} + c$ (with $z = re^{i\varphi}$) has for generic choices of $\alpha > 1/2$ at least 2^{n-1} parameters $c \in \mathbb{C}$ such that 0 is a super-attracting point of (not necessarily prime-)period n. If $\alpha = 1$, then there are exactly 2^{n-1} such parameters.*

Proof. Consider the map $G_n : c \mapsto f_{\alpha,c}^{n-1}(c)$. Obviously G_n is continuous, and it maps, for large R, the circle $\{|c| = R\}$ to a closed curve of radius $\approx R^{(2\alpha)^{n-1}}$ and winding number 2^{n-1} with respect to the origin. Therefore, G_n maps the disk $\{|c| < R\}$ in a 2^{n-1}-fold covering fashion onto a neighborhood of the origin. Therefore, for generic α, $G_n^{-1}(0)$ consists of at least 2^{n-1} points c, and for each such c, $f_{\alpha,c}^n(0) = 0$. If $\alpha = 1$, then

$$f_{1,c}^n(z) = z \text{ for } z = 0 \tag{4}$$

is a polynomial of degree 2^{n-1} over c, hence there are no more than 2^{n-1} solutions. The only possibility that less than 2^{n-1} solutions would occur is when they have multiple multiplicity. For $\alpha = 1$, this does not occur, cf. [9, Theorem VIII 2.1]. For a short

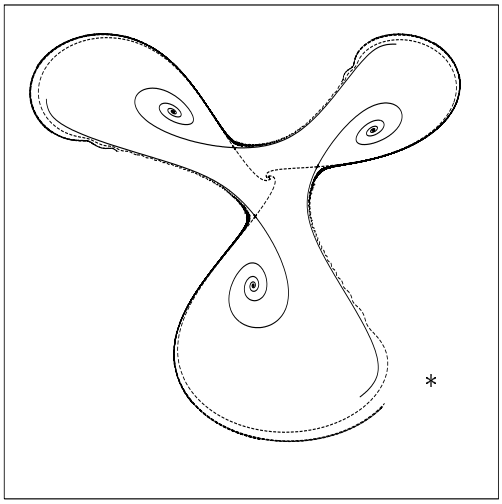

$c = -0.1095 + 0.59i, \quad \alpha = 0.9$

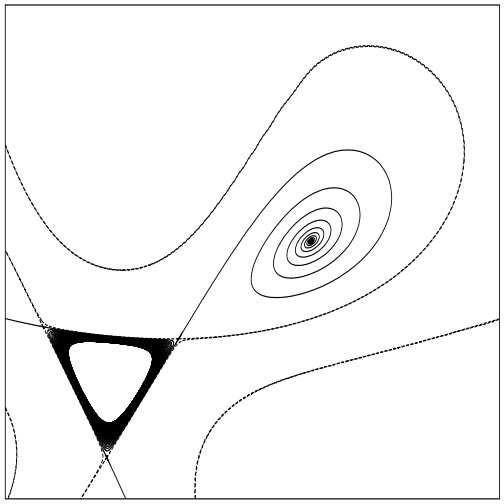

Zoom-in at $c = -0.1095 + 0.5939i$

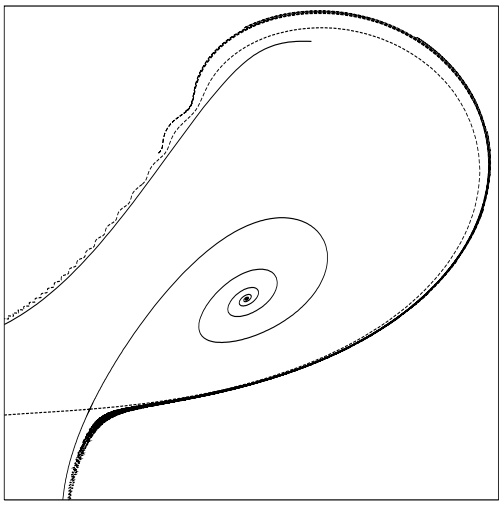

Zoom-in at $c = -0.1095 + 0.59i$

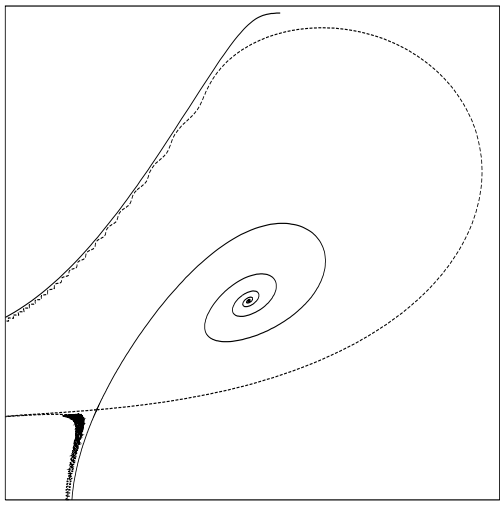

Zoom in at $c = -0.1095 + 0.5896i$

FIGURE 11. Disappearance of a small and appearance of a large invariant circle in a double homoclinic bifurcation. The stable manifold (solid) of the period three saddle orbit crosses both parts of the unstable manifold (dashed).
Top left: Global picture. Top right: Before the the crossings. The invariant circle exists inside the triangle. Bottom left: After the first crossing. No invariant circle exists. Bottom right: After both crossings. A large invariant circle exists.

argument consider (4) over the field $\mathbb{Z}_2[c]$. This equation becomes $c^{2^{n-1}} + c^{2^{n-2}} + \cdots + c^2 + c = 0$, which has no double zeroes over $\mathbb{Z}_2[c]$. □

The Neimarck-Sacker circle at parameters in region 3 of Figure 3 displays resonances, at least for some parameters. We conjecture that these correspond to Arnol'd tongues depicted schematically in Figure 12. The cuspidal tongues, widening to bulbs, can also

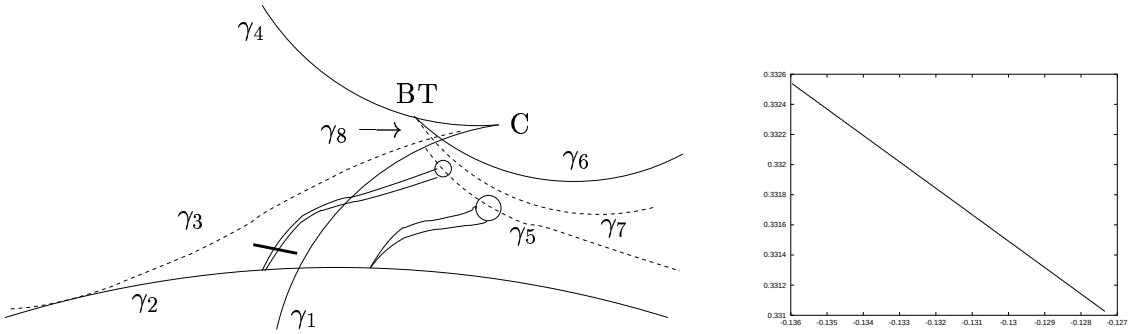

FIGURE 12. Left: Schematic picture of bifurcation curves and Arnol'd tongues near the 1:3 resonance, for $\alpha = 1.1$. The "curves" $\gamma_1, \dots \gamma_6$ are as in Figure 3, γ_7 is the locus where a period 3 Neimarck-Sacker circle (dis)appears due to the critical point and γ_8 is the locus where a period 3 Neimarck-Sacker circle (dis)appears in a homoclinic tangle. Right: Computation of rotation numbers of the Neimarck-Sacker circle for parameter c along the thick arc in the left picture: $\operatorname{Re} c \in [-0.136, -0.127]$ and $\operatorname{Im} c \approx 0.6898$. The bulb on top of each resonance tongue is supposed to contain a parameter where zero is periodic, and hence the narrow region γ_5 should intersect all such bulbs.

been seen in black at the upper rim of the main cardiod in Figure 1, at least for fairly small resonances. For the α-parameters that we have looked at, and c-parameters near the 1:3 resonance point, the tongues are so small, and of such high period, that they are difficult to pinpoint. However, estimates of the rotation number of the Neimarck-Sacker circle show that rational rotation numbers, and hence resonances, do occur in region 3. (The rotation numbers in Figure 12 are computed by estimating the 'slope', by a least square algorithm, of the set $\{(i, F^i(x) - x); i = 0, 1, \dots, N\}$ for $N = 1000$ and F the approximation of the lift of the action on the Neimarck-Sacker circle. This algorithm has a proven error of $\mathcal{O}(1/N^2)$, [7].) In the right half of region 3, these rotation numbers vary between $0.331\dots$ and $0.333\dots$, so the difference with the 1:3 resonance is of $\mathcal{O}(10^{-3})$. This corresponds to resonances of denominator $\mathcal{O}(10^2)$.

For Arnol'd tongues emerging at the lower boundary of region 3 (a subset of curve γ_2), the Neimarck-Sacker circle is shielded off from the critical orbit by the saddle-source connections, see phase portrait 3 of Figure 3. Therefore no such Arnol'd tongue can have its center within region 3. Assuming each tongue is connected, it has to be elongated, curving sideways and crossing the saddle node curve γ_1 into region 6. It is this phenomenon that we illustrate in Figure 12. The Arnol'd tongues are schematic. As far as our numerical evidence goes, it agrees with the observations made by Peckham, see [22, Figure 4f and explanations].

6. A MODEL FOR THE HOLOMORPHIC CASE

Since the family (1) is a perturbation of a holomorphic family, it is natural to ask how the bifurcations presented in this paper behave in the limit to the holomorphic case ($\alpha \to 1$).

In this section we present a holomorphic bifurcation analysis to enable a comparison and to demonstrate how the holomorphic bifurcation diagram (see Figure 13) unfolds to the bifurcation diagrams in Figures 3, 8 and 9. To this end, we derive a model vector field that describes the dynamics of the holomorphic quadratic map near the 1:3 resonance, following the approach of Takens [26]. To be precise, the time-1 flow of this vector field, composed with a rigid rotation, will be conjugate to a perturbation of the map. This perturbation is small near the 1:3 resonance point in the sense that it is of high order in the distance to this point in the combined phase-parameter space. Hence the vector field gives a good qualitative description of the local dynamics, in particular of the relevant periodic points and local bifurcations of the map. The advantage of the model is that such a planar vector field is much easier to study than a planar map, both theoretically and numerically. A bifurcation analysis of the vector field and a discussion of the relation with the dynamics of the map is given in the second part of this section.

The reader is encouraged to compare this analysis with the well-known approaches of Voronin [27] and Camacho [8], which however focus on the phase- rather than parameter space, and give less attention to multipliers close to $e^{2\pi i/3}$.

The model is obtained in three steps. First, the 1:3 resonance point is translated to the origin. At the resonance point, the linear part of the map is equivariant with respect to a rotation S over angle $2\pi/3$. This permits a normalization of the map, taking it to S-equivariant form, of arbitrarily high order in the parameters and phase variables. This map will be of the form

$$z \mapsto S \circ h(z) \text{ , where } h \text{ is near-identity: } h(z) = z + \text{h.o.t.}$$

In the final step we obtain an S-equivariant vector field X such that $X^1 = h$. Here X^t denotes the flow of X over time t. Thus near the 1:3 resonance point, the original map $f_{\alpha,c}$ is locally conjugate to $S \circ X^1$.

A vector field treatment of the nonholomorphic case is in principle possible, yet will need many more low order terms in the normal form $h(z, \bar{z})$, see below. Hence we reserve this issue for future research.

6.1. **Derivation of the model vector field.** Recall that the holomorphic quadratic map is given by $f_c(u) = u^2 + c$, having a 1:3 resonance point (the organizing center) at $u = u_0 := -\frac{1}{4} + \frac{i}{4}\sqrt{3}$, $c = c_0 := -\frac{1}{8} + \frac{3i}{8}\sqrt{3}$. Translating the 1:3 resonance point to the origin is a straightforward computation, and we summarize the result without proof in the following lemma.

Lemma 2. *Let $\varphi : \mathbb{C} \longrightarrow \mathbb{C}$ be a continuous solution of the equation*

$$\varphi(\mu)^2 + e^{2\pi i/3}\varphi(\mu) - \varphi(\mu) + \mu = 0$$

satisfying $\varphi(0) = 0$. Then φ is uniquely defined, holomorphic and invertible on an open neighborhood of $0 \in \mathbb{C}$. By the invertible, holomorphic transformation

$$(u, c) \mapsto (z, \lambda) := (u - u_0 - \varphi(c - c_0), 2e^{-2\pi i/3}\varphi(c - c_0)),$$

defined on an open neighborhood of $(u_0, c_0) \in \mathbb{C} \times \mathbb{C}$, and mapping onto an open neighborhood of $(0, 0) \in \mathbb{C} \times \mathbb{C}$, the map f_c is (locally) conjugate to the map $g = g_\lambda$, given

by

$$g_\lambda(z) = e^{2\pi i/3}\,(1+\lambda)\,z + z^2.$$

Thus we consider the map g near the resonance point $(z,\lambda) = (0,0)$. At $\lambda = 0$, the linear part of g is given by Sz, where $S = e^{2\pi i/3}$ is a rotation over one third of a full circle. Thus this linear part is S-equivariant, and a standard normal form theorem now shows that g can be made S-equivariant up to any order in z by applying near-identity transformations. To be precise, we have the following theorem, compare Appendix A for a proof.

Theorem 1. *Let $N \in \mathbb{N}$, $N > 1$. Then there exists a holomorphic transformation $\psi_N : \mathbb{C} \longrightarrow \mathbb{C}$ such that*

$$\psi_N{}_* g = g_N + O(z^N)\ ,\ \textit{where } S_* g_N = g_N.$$

The map ψ_N depends on λ and is near-identity in the sense that $\psi_N(z) = z + O(z^2)$.

A straightforward normal form calculation shows that, for any $N \geq 10$ and any $M \geq 1$, there exists a transformation $\psi = \psi_{N,M}$ of the above type, such that $\psi_* g(z) = e^{2\pi i/3} h(z)$, where

$$\begin{aligned} h(z) &= z + \lambda z + a(\lambda) z^4 + b(\lambda) z^7 + \lambda^M z^{10} r_\lambda(z) + O(z^N)\ \text{, with} \\ a(\lambda) &= \frac{3}{2} + \frac{i}{6}\sqrt{3} + O(\lambda), \\ b(\lambda) &= -\frac{64}{9} - \frac{16i}{9}\sqrt{3} + O(\lambda). \end{aligned}$$

The holomorphic function r is S-equivariant.

The map h is analytic and near-identity, and hence there exists a vector field X such that h equals the flow of X over time 1: $X^1 = h$, compare Takens [26]. This vector field is of the form

$$X_\mu(z) = \mu z + \tilde{a}(\mu) z^4 + \tilde{b}(\mu) z^7 + O(z^{10}),$$

where $\mu = \log(1+\lambda) = \lambda + O(\lambda^2)$ is a small parameter. We refer to Appendix B for details on the computation. Applying a rotation $z \mapsto \tilde{a}^{1/3} z$ to remove the coefficient in front of the z^4 term, we obtain the vector field

$$X_\mu(z) = \mu z + z^4 + c(\mu) z^7 + O(z^{10}).$$

In this formula the new phase variable is again called z for simplicity, and

$$c(\mu) = \tilde{b}(\mu)(\tilde{a}(\mu))^{-2} = -\frac{1076}{147} - \frac{8i}{147}\sqrt{3} + O(\mu).$$

6.2. **Bifurcation analysis.** In a neighborhood of $(z,\mu) = (0,0)$, the vector field X_μ has at most four equilibria $z = z_j$, $j = 0,1,2,3$, given by

$$z_0 = 0 \text{ and } z_j = -\sqrt[3]{\mu}\left(1 + \frac{1}{3}c(0)\mu + O(\mu^2)\right)\ ,\ j = 1,2,3,$$

where the multivaluedness of the latter expression yields three different equilibria for $\mu \neq 0$. The equilibrium $z = 0$ is stable for $\mathrm{Re}(\mu) < 0$, and unstable for $\mathrm{Re}(\mu) > 0$.

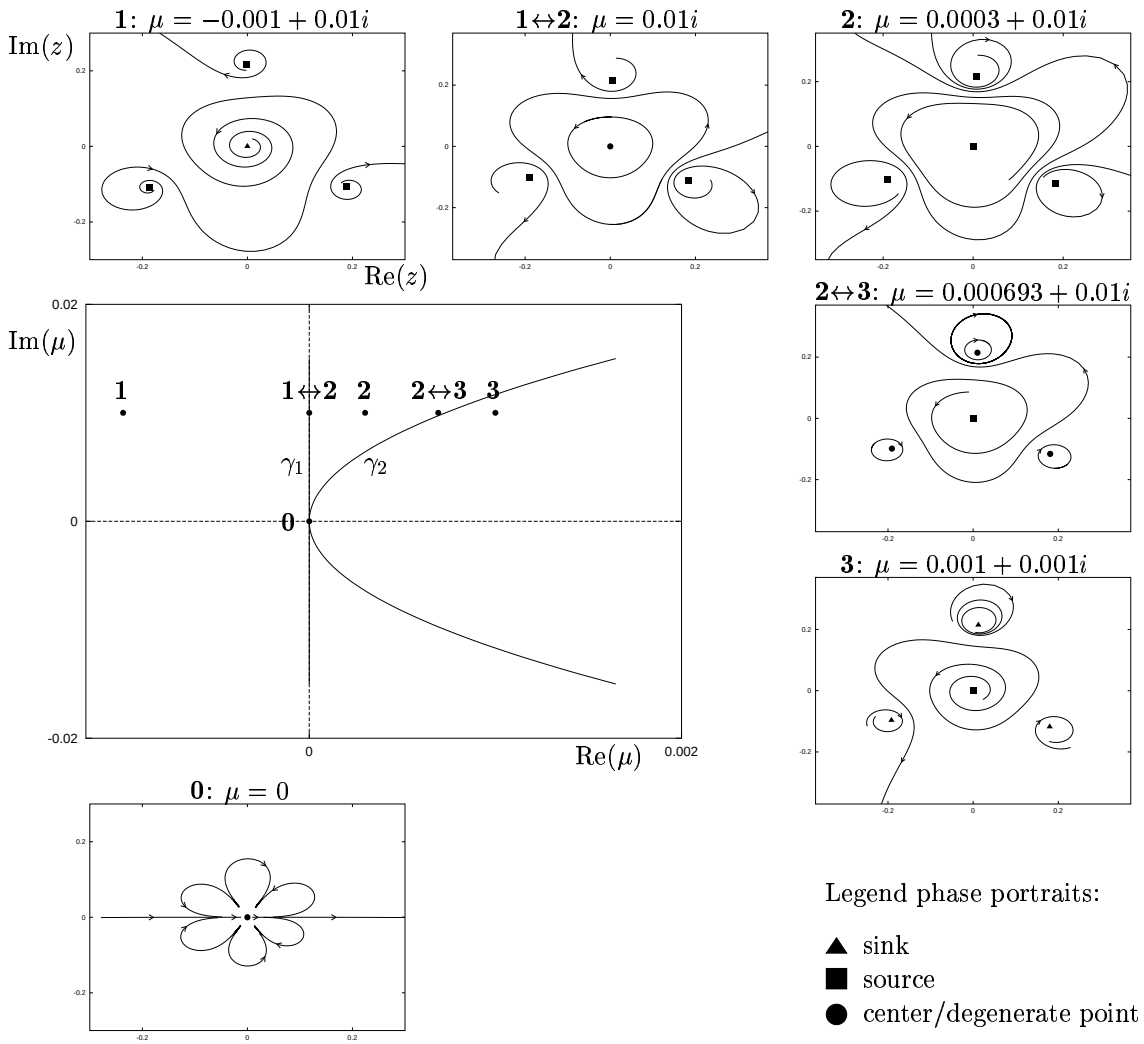

FIGURE 13. Bifurcation diagram and phase portraits of the vector field that models the holomorphic map near the 1:3 resonance point. Phase portraits are located at the indicated parameter points. The dynamics is explained in Section 6.

(We do not distinguish between a node or a focus.) The other equilibria are stable for $\mathrm{Re}(\mu) > u(\mathrm{Im}(\mu))$ and unstable for $\mathrm{Re}(\mu) < u(\mathrm{Im}(\mu))$, where

$$u(t) = -\mathrm{Re}(c(0))t^2 + O(t^3) = \frac{1076}{147}t^2 + O(t^3).$$

Thus there are three regions (labeled 1 – 3) with qualitatively different dynamics in phase space, separated by two curves γ_1: $\mathrm{Re}(\mu) = 0$ and γ_2: $\mathrm{Re}(\mu) = u(\mathrm{Im}(\mu))$. A bifurcation diagram with phase portraits is shown in Figure 13. We note that all phase portraits are S-equivariant. To compute this picture we actually use the vector field $\tilde{X}_\mu(z) = \mu z + z^4 + c(0)z^7$, that equals X_μ apart from a small remainder of order $O(\mu z^7, z^{10})$.

In region 1 the origin is a sink and the other three equilibria are sources. Traversing the curve γ_1 into region 2, z_0 destabilizes, and becomes a source. On the curve γ_1 for $\mu \neq 0$, the origin is a center (i.e., it has purely imaginary eigenvalues), surrounded by a continuous family of closed orbits (this latter remark follows from Schwarz' lemma).

Passing through the curve γ_2 from region 2 into region 3, the equilibria z_1, z_2 and z_3 stabilize. On γ_2 for $\mu \neq 0$ these equilibria are centers and surrounded by invariant closed curves.

Going directly from region 1 to region 3 through $\mu = 0$ all equilibria coincide for $\mu = 0$ and change stability at the same point. Thus, at $\mu = 0$ there is a single degenerate equilibrium, having three attracting and three expanding directions (the figure shows one of each). These correspond to the Leau-Fatou petals known from parabolic fixed points for conformal maps. In general, the number of (attracting or repelling) petals could be any multiple of three, depending on the order of degeneracy. Since each cycle of petals contains a critical point, and the quadratic family has only one critical point in $\mathbb{C}$, there can be only three. By continuity, the same is true for $\alpha \approx 1$.

For the original map g_λ (or f_c) this means the following. It is conjugate to $S \circ X^1$ up to a small perturbation, and hence the nonzero equilibria of X correspond to a period three orbit of g, while the equilibrium at $z = 0$ is just a fixed point. The local bifurcations of the vector field are the same as those of the map, since they are determined completely by the low order terms in z and μ. In this sense, the vector field gives a good description of the local dynamics of the map, i.e., for small z and μ.

Regions 1 and 3 correspond to the main cardioid and the (upper) period three bulb of the Mandelbrot set, respectively, with a single point of contact $\mu = 0$ at the 1:3 resonance. The degenerate vector field at this point corresponds to a Fatou flower. Arbitrarily close to the 1:3 resonance there are other resonance points on the boundary of the main cardioid, but they are not "seen" by the vector field since it is tuned to the 1:3 resonance (that is, only points of period *three* correspond to equilibria of the vector field).

To allow a better comparison with the nonholomorphic bifurcation analysis, let us add a table indicating which curves and regions correspond to which in the three bifurcation diagrams.

Figure 3	Figures 8 and 9	Figure 13
γ_2	γ_3	γ_1
γ_6	$\gamma_4 \cup \gamma_6$	γ_2
region 1	region 1	region 1
region $6 \cup 7$	region 11	region 2
region 5	region 9	region 3

Appendix A. A normal form theorem

In this appendix we prove that the map $g : z \mapsto e^{2\pi i/3}(1+\lambda)\, z + z^2$ is locally conjugate to a map of the form

$$z \mapsto e^{2\pi i/3}\left(z + \lambda z + a(\lambda) z^4 + b(\lambda) z^7\right) + \lambda^M z^{10} r_\lambda(z) + O(z^N), \tag{5}$$

for any $M \geq 1$ and $N \geq 10$. For a detailed statement, see Section 6. First we show that any term $a(\lambda)z^k$ in the expansion of g can be transformed away, provided that $k-1$ is not a multiple of 3. Then we show that the remaining terms can be brought to the given form, i.e., that they are of order M in λ, except for the terms z^4 and z^7.

Consider a map of the form

$$f(z) = e^{2\pi i/3}(1+\lambda)z + p_\lambda(z) + a(\lambda)z^m + O(z^{m+1}), \tag{6}$$

where $m - 1 \bmod 3 \neq 0$ and p_λ is S-equivariant, i.e.,

$$p_\lambda(z) = \sum_{j\geq 1, 3j<m} c_j(\lambda) z^{3j+1}.$$

Note that the map g is of this form, with $p = 0$, $m = 2$ and $a = 1$.

We want to kill the term $a(\lambda)z^m$. Consider a local holomorphic transformation of the form $\psi(z) = z + d(\lambda)z^m$. Then (recalling that S is the rotation over $2\pi/3$)

$$\begin{aligned} \psi \circ f \circ \psi^{-1}(z) &= e^{2\pi i/3}(1+\lambda)z + p_\lambda(z) + a(\lambda)z^m \\ &+ d(\lambda)\left((1+\lambda)^m S^m - (1+\lambda)S\right) z^m + O(z^{m+1}). \end{aligned}$$

Since $(1+\lambda)^m S^m - (1+\lambda)S = S^m - S + O(\lambda) \neq 0$ for λ sufficiently small, we can take

$$d(\lambda) = -\frac{a(\lambda)}{(1+\lambda)^m S^m - (1+\lambda)S},$$

and hence

$$\psi \circ f \circ \psi^{-1}(z) = e^{2\pi i/3}(1+\lambda)z + p_\lambda(z) + O(z^{m+1}),$$

which is again a map of the form (6), for a larger value of m.

Starting with the map g and proceeding inductively with respect to m, we can thus kill all non-S-equivariant terms in g, resulting in a map of the form

$$f(z) = e^{2\pi i/3}(1+\lambda)z + a(\lambda)z^4 + b(\lambda)z^7 + p_\lambda(z) + O(z^N),$$

where $p_\lambda(z) = \sum_{j\geq 3, 3j+1<N} c_j(\lambda) z^{3j+1}$. A direct calculation shows that $a(0) \neq 0$ in our case.

It is to be shown that f is conjugate to a map of the same form where all the c_j's are of order M in λ. We proceed by a double induction, in the outer loop with respect to the order in λ, and in the inner one with respect to the order in z, that is, with respect to j. Thus, let us assume that c_j is of order $m+1$ in λ for all $j \in \{3, 4, \ldots, n-1\}$ $(n \geq 3)$, while c_j is only of order m for $j \geq n$. Let ψ be the parameter-dependent transformation

$$\psi(z) = z + d(\lambda)z^{3(n-1)+1},$$

then a tedious but straightforward calculation shows that

$$\begin{aligned}\psi \circ f \circ \psi^{-1}(z) &= e^{2\pi i/3}\,(1+\lambda)\,z + a(\lambda)z^4 + b(\lambda)z^7 \\ &+ \sum_{j=3}^{n-2} c_j(\lambda) z^{3j+1} + \left(c_{n-1}(\lambda) + d(\lambda)q(\lambda)\right) z^{3(n-1)+1} \\ &+ \Big(c_n - 4a(\lambda)d(\lambda) + (3n-2)(1+\lambda)^{3(n-1)} a(\lambda)d(\lambda)\Big)\, z^{3n+1} \\ &+ \sum_{j>n} c_j(\lambda) z^{3j+1} + d(\lambda) z^{3(n+1)+1} r_\lambda(z^3) + O(z^N),\end{aligned}$$

where r is some holomorphic function, and

$$q(\lambda) = e^{2\pi i/3}(1+\lambda)\left((1+\lambda)^{3(n-1)} - 1\right).$$

Since $a(0) \neq 0$ and $n \geq 3$, we can choose (for sufficiently small λ)

$$d(\lambda) = -\frac{c_n}{\left((3n-2)(1+\lambda)^{3(n-1)} - 4\right) a(\lambda)} = O(\lambda^m),$$

such that the transformed map becomes

$$\psi \circ f \circ \psi^{-1}(z) = e^{2\pi i/3}\,(1+\lambda)\,z + a(\lambda)z^4 + b(\lambda)z^7 + \sum_{j\geq 3} \tilde{c}_j(\lambda) z^{3j+1} + O(z^N).$$

Here $\tilde{c}_j = c_j$ for $3 \leq j < n-1$, $\tilde{c}_n = 0$, and $\tilde{c}_j = c_j + O(\lambda^m)$ for $j > n$, absorbing terms of r_λ. From $q(\lambda) = O(\lambda)$ it follows that $\tilde{c}_{n-1} = c_{n-1} + d(\lambda)q(\lambda) = O(\lambda^{m+1})$. Hence this transformation takes us one step further in the induction process.

To conclude, we note that a final number of holomorphic local transformations is needed to obtain the final form (5). The coefficients $a(0)$ and $b(0)$ as stated in Section 6 are obtained by a straightforward calculation. Applying infinitely many transformations, one can push the numbers M and N to infinity. However, the resulting composed transformation is in general not analytic, and an infinitely flat remainder will remain in (5). For a local bifurcation analysis, finite values of M and N are sufficient.

Appendix B. The analytic vector field

Given the near-identity map h defined in Section 6, we show how to obtain a vector field X such that $X^1 = h$. Recall that h is of the form

$$h(z) = z + \lambda z + a(\lambda)z^4 + b(\lambda)z^7 + \lambda^M z^{10} r_\lambda(z) + O(z^N),$$

for some functions a, b and r. Consider a vector field X of the form

$$X_\mu(z) = \mu z + \tilde{a}(\mu)z^4 + \tilde{b}(\mu)z^7 + O(z^{10}),$$

where μ is some small parameter. We want to determine $\tilde{a}$ and $\tilde{b}$ such that $X^1 = h$. The time-1 flow X^1 is given by

$$\begin{aligned}X^1 &= \sum \frac{1}{n!} X_n \text{ , where} \\ X_1 &= X(z), \\ X_n &= X(X_{n-1}) \text{ for } n > 1.\end{aligned}$$

Here X is considered as a directional derivative, and z denotes the coordinate function on z. Thus X_n is the n-fold action of X on z: $X_n = XX\dots X(z)$, and the expansion simply expresses the fact that X^1 is the exponential of X.

Using this formula, a straightforward calculation shows that

$$X^1 = e^\mu z + \tilde{a}(\mu)z^4 + \left(\tilde{b}(\mu) + 4\tilde{a}^2(\mu)\right) z^7 + O(\mu z^4, z^{10}).$$

Thus we should take $\mu = \log(1+\lambda)$, and $\tilde{a}$, $\tilde{b}$ have to satisfy

$$\begin{aligned} \tilde{a}(0) &= a(0) = \frac{3}{2} + \frac{i}{6}\sqrt{3}, \\ \tilde{b}(0) &= b(0) - 4a^2(0) = -\frac{142}{9} - \frac{34i}{9}\sqrt{3}. \end{aligned}$$

Appendix C. External rays

In this appendix we briefly explain how to construct external rays in the basin $A(\infty)$ of the point at infinity, i.e., we construct a bijection $h : A(\infty) \to \{z \ ; \ |z| > 1\}$ such that $h \circ f_{\alpha,c} = h^2(z)$. The *external ray* of *external angle* ϑ is the curve $R_\vartheta := h^{-1}(\{re^{2\pi i\vartheta} \ ; \ r > 1\})$.

Assume that $c \in \mathcal{M}_\alpha$. First extend $f_{\alpha,c}$ to a two-fold cover of the Riemann sphere $\overline{\mathbb{C}}$. The point ∞ is super-attracting and slight adaptations of standard approaches yields a conjugacy to the map $z \mapsto z^2$ on $\overline{\mathbb{C}}$. Indeed, define the Green function as

$$G(z) = \left(\log \lim_{n\to\infty} |f^n_{\alpha,c}(z)|^{1/(2\alpha)^n}\right)^\kappa,$$

for $\kappa = \log 2/\log(2\alpha)$. Then $G(z)$ is well defined om $A(\infty)$, takes values in $(0,\infty)$ and satisfies $G(f(z)) = 2G(z)$. The level curves $G_K = \{z \mid G(z) = K\}$ are the Green lines. They are topological circles, and $\partial A(\infty) = \lim_{K\to 0} G_K$ is called the Caratheodory loop.

For large K, the region $A_K := \{z \mid K \le G(z) < 2K\}$ is an annulus, and the subsets $A_{K,i} = \{z \in A_K \mid \text{Re } f^j(z) > 0 \text{ for } 0 \le j \le i\}$ are nested (half-open) topological disks whose intersection $C_K = \cap_{i\ge 0} A_{K,i}$ connects the two boundary curves of A_K. Any small disk $D = B(z;\varepsilon)$ for $|z|$ large expands under iteration of $f_{\alpha,c}$ to contain a large annular region around ∞. Therefore, if $\partial D \cap C_K$ contains at least three points, then at least one arc $H \subset \partial D$ connecting two of those points will not remain in $\{z \ ; \ Re(z) > 0\}$. Therefore C_K is an arc. The union $R_0 = \cup_{K>0} C_K$ is the external ray at angle 0.

As $c \in \mathcal{M}_\alpha$, f^{-1} has two disjoint inverse branches on $A(\infty)$. Based on R_0, we find other external rays, e.g., $R_{1/2} = f^{-1}(R_0)\setminus R_0$ and $f^{-1}(R_{1/2}) = R_{1/4} \cup R_{3/4}$, etc. The dyadic rays give a lamination of $A(\infty)$ and $A(\infty)\setminus\{\text{dyadic rays}\}$ has empty interior, because, as before, any open ball in this interior expands to contain an annular region around ∞. Therefore, by dyadic approximation, we can find the external ray of any angle $\vartheta \in [0,1)$ and all the rays are indeed the bijective copies of $(0,1)$. The map $h(z) = \exp(G(z) + 2\pi i \text{ ext. angle}(z))$ is the required conjugacy satisfying $h \circ f(z) = (h(z))^2$.

If the external ray R_0 has a single *landing point*, i.e., $\lim_{r\searrow 1} h^{-1}(r)$ consist of a single point, then this point is fixed; we call it p'. On the other hand, if $\partial A(\infty)$ contains a hyperbolically repelling fixed point, then an external ray is indeed expected to land at it.

At first glance, the dynamics on the "Caratheodory loop" $\partial A(\infty)$ should be considered as a factor map of the angle doubling map $z \to z^2$ on $\{|z| = 1\}$. At certain regions near the 1:3-resonance, for instance in region 5 of Figure 3 or region 9 of Figure 8, the factor map $h : \{|z| = 1\} \to \partial A(\infty)$ squeezes the period 3 orbit $\{e^{2\pi i/7}, e^{4\pi i/7}, e^{8\pi i/7}\}$ to a single (central) fixed point p of $f_{\alpha,c}$, while the preimage triples of the period 3 orbit are squeezed to preimages of p. It is also possible that the rays of these angles accumulate on more complicated continua, such as invariant circles carrying an (ir)rational rotation, cf. region 10 of Figure 8.

Equally standard geometric arguments show that K_c consists of infinitely many components if $c \notin \mathcal{M}_\alpha$ or equivalently $0 \in A(\infty)$. Note however, that due to the occurrence of saddle points and Neimarck-Sacker circles, these components need not be singletons, so K_c need not be a Cantor set.

References

[1] V. I. Arnol'd, *Geometrical methods in the theory of ordinary differential equations,* Springer, New York, (1983).

[2] D. Aronson, M. Chory, G. Hall, R. McGehee, *Bifurcations from an invariant circle for two-parameter families of maps of the plane: a computer-assisted study,* Comm. Math. Phys. **83** (1982) 303–354.

[3] A. Back, J. Guckenheimer, M. R. Myers, F. J. Wicklin, P.A. Worfolk, *DsTool: Computer assisted exploration of dynamical systems,* Notices Amer. Math. Soc. **39** (1992) 303–309.

[4] B. Bielefeld, S. Sutherland, F. Tangerman, J. Veerman, *Dynamics of certain nonconformal degree-two maps of the plane,* Experiment. Math. **2** (1993) 281–300.

[5] H.W. Broer, R. Roussarie, C. Simó, *Invariant circles in the Bogdanov-Takens bifurcation for diffeomorphisms,* Ergodic Theory Dynam. Systems **16**(6) (1996) 1147–1172.

[6] H. Broer, C. Simó, R. Vitolo, *Bifurcations and strange attractors in the Lorenz-84 climate model with seasonal forcing,* Nonlinearity **15** (2002) 1205–1267.

[7] H. Bruin, *Numerical determination of the continued fraction expansion of the rotation number,* Physica D **59** (1992) 158-168.

[8] C. Camacho, *On the local structure of conformal mappings and holomorphic vector fields in C^2,* Journées Singulières de Dijon (Univ. Dijon, Dijon, 1978), 83–94, Astérisque, 59-60, Soc. Math. France, Paris, (1978).

[9] L. Carleson, Th. Gamelin, *Complex dynamics,* Universitext: Tracts in Mathematics. Springer-Verlag, New York (1993).

[10] E. Doedel, H. B. Keller, J.-P. Kernévez, *Numerical analysis and control of bifurcation problems. I. Bifurcation in finite dimensions,* Internat. J. Bifur. Chaos Appl. Sci. Engrg. **1**(3) (1991) 493–520.

[11] E. Doedel, H. B. Keller, J.-P. Kernévez, *Numerical analysis and control of bifurcation problems. II. Bifurcation in infinite dimensions,* Internat. J. Bifur. Chaos Appl. Sci. Engrg. **1**(4) (1991) 745–772.

[12] A. Douady, *The topological entropy of unimodal maps,* in Real and Complex Dynamical Systems, Conference Proceedings, (Ed. B. Branner and P. Hjorth) Kluwer Acad. Publ. (1995).

[13] C. E. Frouzakis, L. Gardini, I. G. Kevrekidis, G. Millerioux and C. Mira, *On some properties of invariant sets of two-dimensional noninvertible maps*, Internat. J. Bifur. Chaos Appl. Sci. Engrg. **7**(6) (1997) 1167-1194.

[14] C. Frouzakis, I. Kevrekidis, B. Peckham, *A route to computational chaos revisited: noninvertibility and the breakup of an invariant circle,* Physica D **177** (2003) 101-121.

[15] M. Herman, *Are there critical points on the boundaries of singular domains?,* Comm. Math. Phys. **99**(4) (1985) 593–612.

[16] A. Homburg, *Some global aspects of homoclinic bifurcations of vector fields,* PhD thesis, University of Groningen (1993).

[17] Y. Jiang, *Dynamics of certain non-conformal semigroups*, Complex Variables **22** (1992) 27–34.

[18] B. Krauskopf, H.M. Osinga, *Investigating torus bifurcations in the forced van der Pol oscillator,* in Numerical methods for bifurcation problems and large-scale dynamical systems (Minneapolis, MN, 1997), IMA Vol. Math. Appl. **119** (2000) 199–208.
[19] Y. Kuznetsov, *Elements of applied bifurcation theory,* Springer, New York (1995).
[20] John Milnor, *Dynamics in one complex variable. Introductory lectures,* Friedr. Vieweg & Sohn, Braunschweig (1999).
[21] C.H. Nien, *The dynamics of planar quadratic maps with nonempty bounded critical set,* Int. J. of Bif. and Chaos, **8** (1998), 95-105.
[22] B. Peckham, *Real perturbations of complex analytic families: points to regions,* Intern. J. Bifur. & Chaos **8** (1998) 73–93.
[23] B. Peckham, J. Montaldi, *Real continuations from the complex quadratic family: fixed-point bifurcation sets,* Intern. J. Bifur. & Chaos **10** (2000) 391–414.
[24] E. Sander, *Hyperbolic sets for noninvertible maps and relations,* Discrete Contin. Dynam. Systems **5** (1999) 339–357.
[25] J. Szcryzek, *Hausdorff dimension of a limit set for a family of nonholomorphic perturbations of* $z \mapsto z^2$, Nonlinearity **12** (1999) 1439–1448.
[26] F. Takens, *Forced oscillations and bifurcations,* in Applications of global analysis I (Sympos., Utrecht State Univ., Utrecht, 1973), Comm. Math. Inst. Rijksuniv. Utrecht **3** (1974) 1–59. Reproduced in *Global analysis of dynamical systems – Festschrift dedicated to Floris Takens for his 60th birthday*, 1–61. Institute of Physics Publishing, 2001.
[27] S. M. Voronin, *Analytic classification of germs of conformal mappings* $(\mathbb{C}, 0) \to (\mathbb{C}, 0)$, Funktsional. Anal. i Prilozhen. **15** (1981) 1–17.

University of Surrey, School of Electronics and Physical Sciences, Department of Mathematics and Statistics, Guildford, Surrey GU2 7XH, UK

E-mail address: H.Bruin@surrey.ac.uk

URL: http://www.maths.surrey.ac.uk/showstaff?H.Bruin

School of Mathematics, Georgia Institute of Technology, Atlanta, GA 30332, USA

E-mail address: martijn@math.gatech.edu

URL: http://www.math.gatech.edu/~martijn/